Azimuthal velocity analysis of 3D seismic for fractures: Altamont-Bluebell field

Khaled Al Dulaijan and Gary F. Margrave

ABSTRACT

Altamont-Bluebell field is located in northeastern Utah within the Uinta basin. The Uinta basin is an asymmetric east-west trending basin with a south flank that has a gentle slope. The north flank is steep and bounded by east-west trending Uinta Mountains. The field is located in the northern-central part of the basin. In 2010, a 3D surface seismic survey was acquired over 35 square miles area within Bluebell Field, the eastern portion of Altamont-Bluebell field. The Bluebell field is considered an unconventional reservoir in the sense that natural fractures act as fluid storage and conduits in the tight sandstones, shales, and carbonates. Information related to fracture orientation and intensity is vital for the development of such reservoirs. Azimuthal variations of P-wave velocities can be a valuable tool for information related to fractures. Therefore, this paper utilizes Velocity Variations with Azimuth (VVAZ) to estimate the direction and intensity of fracture-induced anisotropy within Upper Green River, Lower Green River, and Wasatch/Colton formations.

A method for VVAZ inversion, based on the elliptical NMO equation for Transverse Isotropy (TI) media that was derived by Grechka and Tsvankin (1998), is applied. The method has been tested on a 3D physical modeling dataset. The results of the physical modeling test are found to be adequate (Al Dulaijan et. al., 2015). For Bluebell field 3D seismic data, isotropic velocities are used along with azimuthally variant time residuals to estimate fast and slow NMO velocities and their directions. Along with fast and slow NMO velocity maps, maps of fracture-induced anisotropy orientation and intensity were created. Dix-type interval properties are calculated to estimate interval anisotropy for each reservoir interval. Pre-stack and post-stack seismic attributes are also calculated for the Upper Green River formation in Bluebell field and compared to VVAZ results. Intensity and orientation maps of seismic anisotropy are compared to post-stack coherency attributes and to geomechanical attributes obtained by seismic pre-stack elastic inversion to estimate brittle zones of the unconventional reservoir.

INTRODUCTION

Altamont- Bluebell field is located in northeastern Utah in the Uinta basin. The Uinta basin is an asymmetric east-west trending basin with a south flank that slopes gently. The north flank is bounded by east-west trending Uinta Mountains. The Bluebell-Altamont field is located in the northern-central part of the basin (Figure 1). Production is from Tertiary sandstones, shales and carbonates. There are three main targets in the field: Upper Green River, Lower Green River, and Wasatch/Colton (Lynn et. al, 1995).

The strata were deposited in lacustrine and alluvial environments. The Upper Green River formation was deposited in open-lacustrine and most of the kerogen is immature. Gas may be migrated from deeper formations. The Lower Green River formation was deposited in marginal and open lacustrine. The kerogen-rich shale and marlstone are the sources of oil. Lastly, Colton formation is alluvial and its source of oil is the Kerogen-rich shale. It is a highly overpressured reservoir as a result of hydrocarbon generation. The hydrocarbon generation in the deep Colton formation is the main cause for natural fractures. Natural fractures in the shallower Green River reservoirs are tectonically induced (Morgan et. al., 2003).

Bluebell-Altamont field is unconventional in the sense that natural fractures act as storage and conduits in the tight sandstones and carbonates. Bluebell field is the eastern portion of the Bluebell-Altamont field. Its cumulative production is 336 MMBO, 588 BCFG, and 701 MMBW. The objective of this study is to identify density and direction of fractures to help in determining well spacing to existing wells needed to effectively drain the remaining hydrocarbon reserves in the Bluebell field, and to identify new drilling opportunities (Adams et. al, 2014).

SEISMIC DATA ACQUISTION AND PROCESSING

3D seismic is acquired over an area of 35 square miles within Bluebell field in 2010. Figure 2 shows a basemap of 3D seismic data, with color indicating fold. Two vibrators were used for each shot and an array of six geophones over a 6' circle were used for each channel. The receiver and source intervals are 220'. The receiver lines are oriented E-W and spaced 1100', while source lines are oriented N-S and spaced 660'. Bin size is 110'x110', and the nominal fold is 240. In addition, a zero-offset VSP survey location is indicated by a black circle.

Refraction statics were applied. Heavy noise were observed and suppressed in multiple domains (i.e., shot, CDP, inline-azimuth-shot line). Also, spherical divergence correction, surface-consistent amplitude corrections, and deconvolution were applied. The zero-offset VSP is used to calculate Q that later was accounted for in the 3D seismic data. Isotropic velocity analysis at one-mile interval and NMO corrections were followed by residual statics. Second pass of velocity analysis at half-mile interval were followed by another pass of residual statics. After muting, data is stacked.
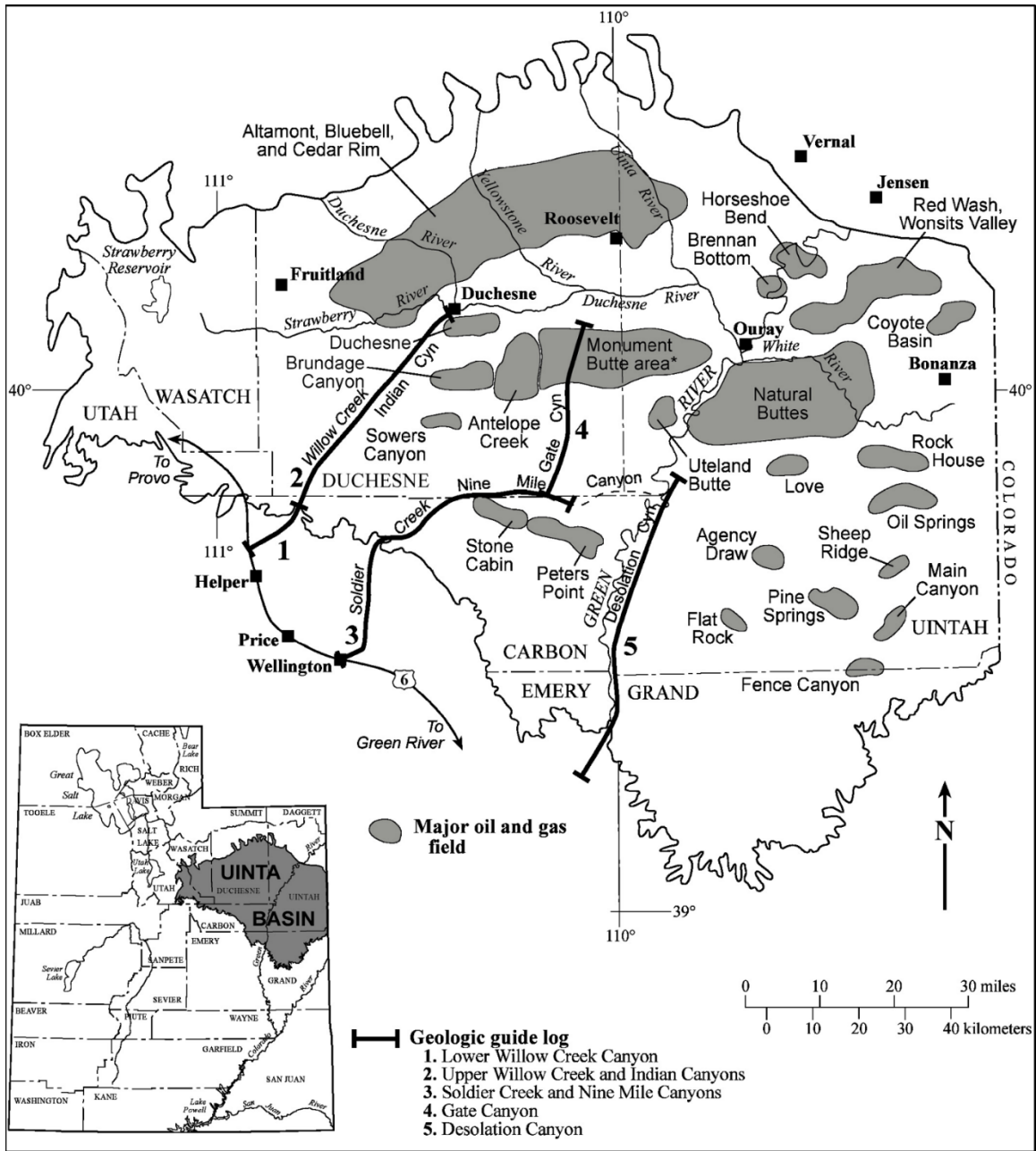
Fig. 1. Location of Uinta basin, Utah (bottom left) and major oil and gas fields within Uinta basin (after Morgan, 2003).

Prior to PSTM, data were binned into Common Offset Vector (COV). COV allows azimuthal information to be preserved after PSTM. Isotropic migration is preformed and followed by VTI analysis, and VTI PSTM. PSTM inline stacks intersecting the VSP are shown in Figure 3 with the reference to the base map (bottom right).

SEISMIC DATA ANALYSIS

Top of Upper Green River formation and Mahogany bench are picked and indicated by blue and green respectively on the stacked sections in Figure 3. Upper Green River consists of lacustrine carbonate and clay, while Mahogany bench consists of shale and is a very strong marker (Lucas and Drexler, 1976). Mahogany bench is within the Upper Green River formation. The fracture analysis carried in this paper is on the interval from Upper Green River top to Mahogany bench.

Unlike Amplitude Variations with Azimuth AVAz methods, VVAz methods use base of the target rather than top of the target. The base of the target, the top of Mahogany bench, traveltimes are displayed along the post-stack seismic volume in Figure 4. The Mahogany bench traveltimes are shallowest in the northeastern and southwestern part of the survey. Isochron map indicating the thickness of the reservoir from top of Upper Green River to Mahogany Shale is shown in Figure 5. The reservoir thickens at southwest part. At the three main targets, largest incident angles, that can be analyzed, are between 30° to 40°, as shown by Figure 6.
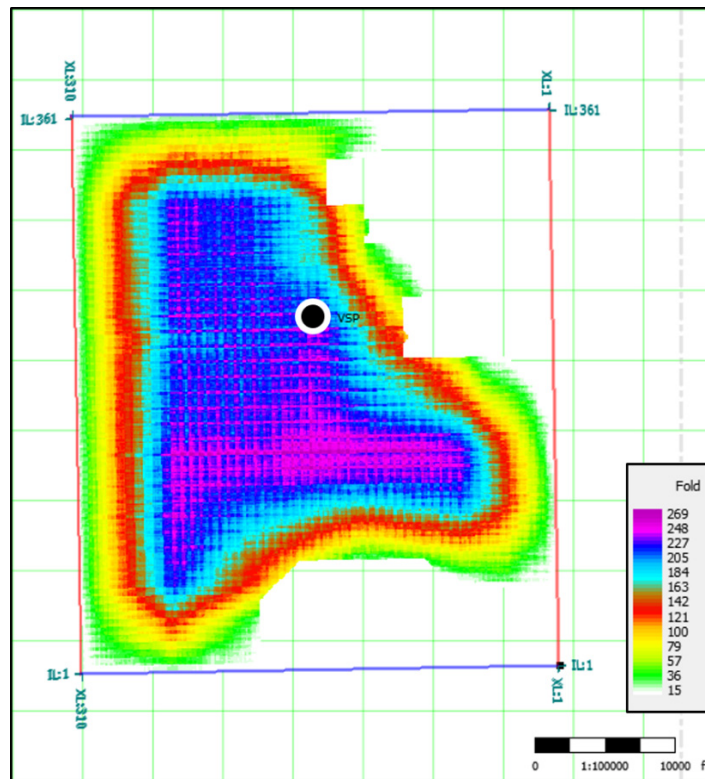

Fig. 2 A basemap of 3D seismic data. Color indicates fold of 110'x110' bins. VSP location is indicated by black circle.
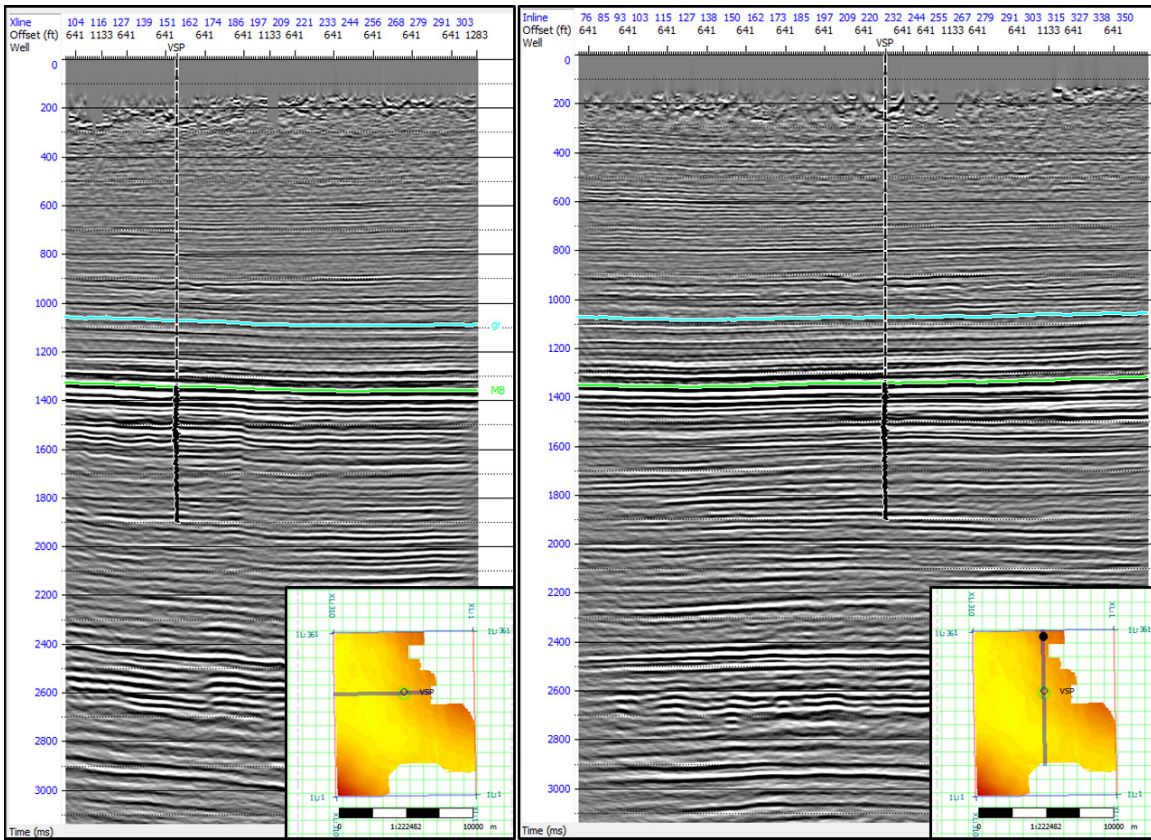
Fig 3. CDP Stack: inline (left) and crossline (right). VSP borehole is indicated in the middle and basemap in the bottom right. Two horizons are indicated Upper Green River (blue) and Mahogany bench (green)
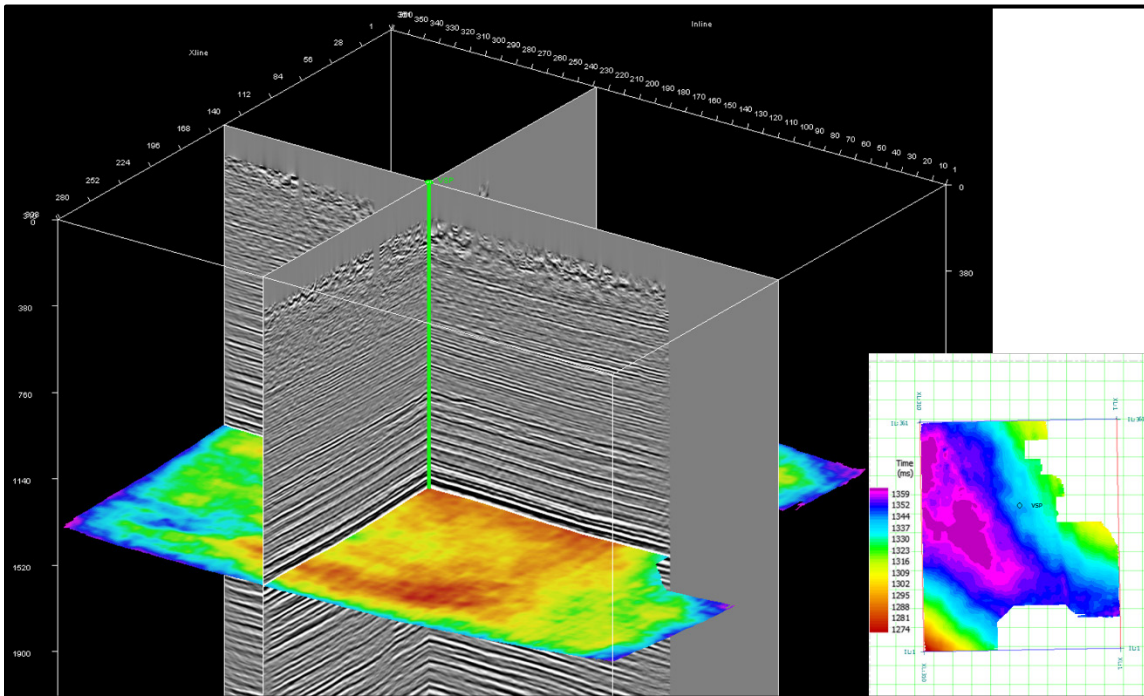

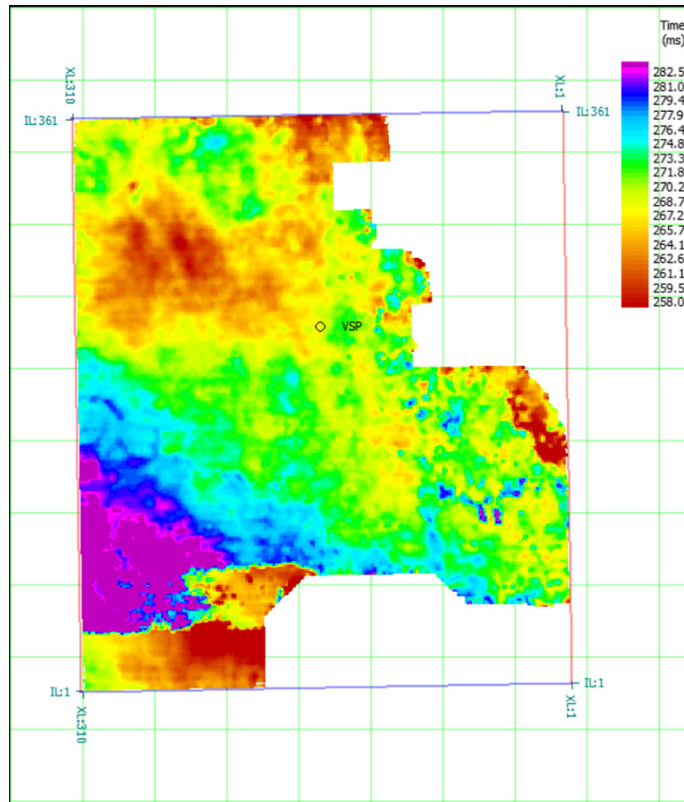Fig 4. Mahogany bench indicated on seismic volume. Green line indicates VSP.

Fig. 5. Isochron indicating the thickness of the reservoir from top of Upper Green River to Mahogany Shale. The reservoir thickens at southwest part.
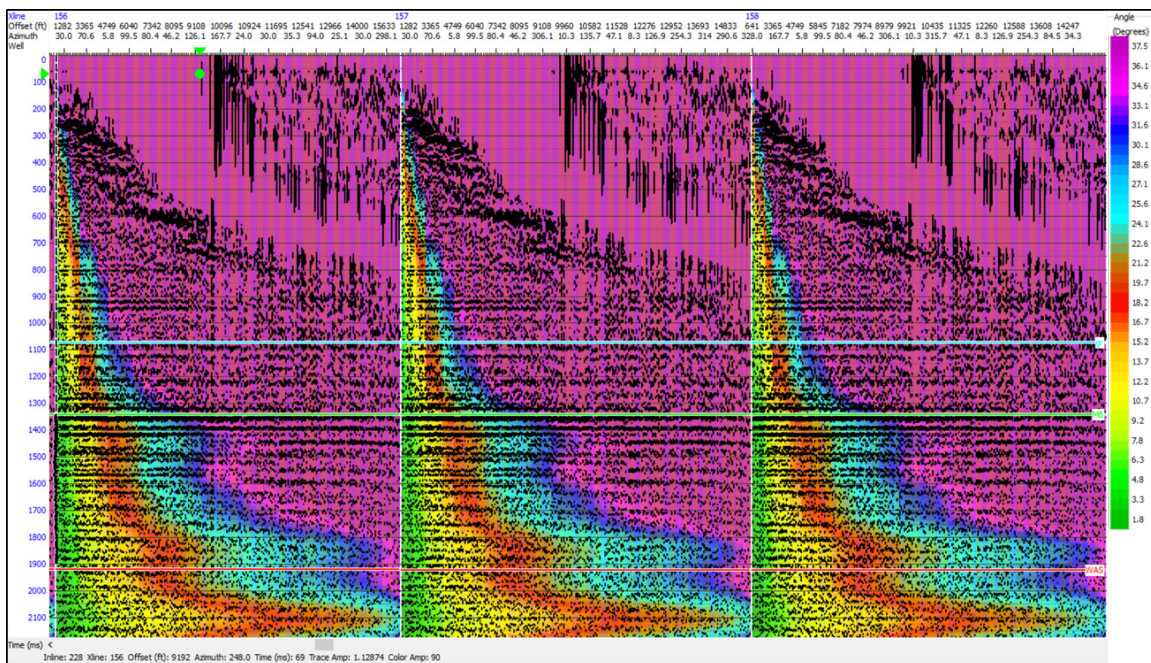

Fig. 6. PSTM image Gather (COV). Color indicates angle of incidences. At target levels, maximum angles are 30º to 40º.

VELOCITY VARIATIONS WITH AZIMUTH

Grechka and Tsvankin (1998) showed that azimuthal variations of NMO velocities can be estimated by an ellipse in the horizontal plane under four assumption. First, the medium is arbitrarily anisotropic and inhomogeneous, so the azimuthal variations in traveltimes are smooth function of surface locations. Second, traveltimes exist at all azimuth. A case of salt domes creating a shadow zone at a specific azimuth violates the second assumption. Third assumption is routinely assumed in seismic data processing steps, such as CMP binning and stacking. That is traveltimes can be described by a Taylor series expansion of $t^2 x_\phi^2$, where t and x_ϕ are traveltimes and source-receiver offset at specific azimuth. Lastly, traveltimes increase with offset at all azimuths. Those assumptions are nonrestrictive in most cases. Grechka and Tsvankin (1998) derived an elliptical NMO equation for TI media where source-receiver offset do no exceed the depth of the reflector. Hyperbolic NMO can be approximated by:

$$T^2 = T_0^2 + \frac{x^2}{V_{NMO}^2(\phi)} \tag{1}$$

, where

$$\frac{1}{V_{NMO}^2(\phi)} = \frac{1}{V_{slow}^2} cos^2(\phi - \beta_s) + \frac{1}{V_{fast}^2} sin^2(\alpha - \beta_s) \tag{2}$$

, where T is the total two-way traveltimes, T_0 is the zero-offset two-way traveltimes. x is the offset, V_{fast} and V_{slow} are the fast and slow NMO velocities respectively. β_s is the azimuth of the slow NMO velocity, while $V_{NMO}(\phi)$ is the NMO velocity as function of the source-receiver azimuth (Figure 7).

Equation (2) can be written as:

$$\frac{1}{V_{NMO}^2(\phi)} = W_{11} \cos^2(\phi) + 2W_{12} \cos(\phi) \sin(\phi) + W_{12} \sin^2(\phi) \tag{3}$$

, where W_{11}, W_{12}, and W_{22} are the ellipse coefficients that are related to the slow and fast NMO velocities and to the azimuth of the slow NMO velocity by

$$\frac{1}{V_{fast}^2} = \frac{1}{2}[W_{11} + W_{22} - \sqrt{(W_{11} - W_{22})^2 + 4W_{12}^2} \tag{4}$$

$$\frac{1}{V_{slow}^2} = \frac{1}{2}[W_{11} + W_{22} + \sqrt{(W_{11} - W_{22})^2 + 4W_{12}^2} \tag{5}$$

$$\beta_s = \tan^{-1} \frac{W_{11} - W_{22} + \sqrt{(W_{11} - W_{22})^2 + 4W_{12}^2}}{2W_{12}} \tag{6}$$

The azimuth of the fast velocity is 90° away from the azimuth of the slow velocities as shown by Figure 7 (Jenner, 2001). The total travel can be written as:

$$T^2 = T_0^2 + x^2 \cos^2(\phi)W_{11} + 2x\,cos(\phi)\sin(\phi)W_{12} + x^2\sin^2(\phi)W_{22}. \quad (7)$$

Equation (7) can be written as:

$$d = Gm\,,$$

where d is n-dimensional data vector, m is the 6-dimensionl model parameter vector, and G is the n-by-4 data kernel as:

$$\begin{pmatrix} T_1^2 \\ T_2^2 \\ \vdots \\ T_n^2 \end{pmatrix} = \begin{pmatrix} 1 & x_1^2\cos^2(\phi_1) & 2x_1\,cos(\phi_1)\sin(\phi_1) & x_1^2\sin^2(\phi_1) \\ 1 & x_1^2\cos^2(\phi_1) & 2x_1\,cos(\phi_1)\sin(\phi_1) & x_1^2\sin^2(\phi_1) \\ \vdots & \vdots & \vdots & \vdots \\ 1 & x_{n1}^2\cos^2(\phi_n) & 2x_1\,cos(\phi_1)\sin(\phi_1) & x_1^2\sin^2(\phi_1) \end{pmatrix} \begin{pmatrix} T_0^2 \\ W_{11} \\ W_{12} \\ W_{22} \end{pmatrix}. \quad (8)$$

Isotropic NMO velocities V_{NMO} and zero-offset traveltimes T_0 are used along with azimuthally variant time residuals, dT_ϕ to estimate azimuthal traveltimes, T, as follows:

$$T = T_x + dT_\phi \quad (9)$$

, where

$$T_x = \sqrt{T_0^2 + \frac{x^2}{V_{NMO}{}^{\wedge}2}} \quad (10)$$

For Dix-type interval ellipse coefficients, W_l, we use the Grechka et. al., 1999 relation:

$$W^{-1}{}_l = \frac{T_0(l)W^{-1}(l) - T_0(l-1)W^{-1}(l-1)}{T_0(l) - T_0(l-1)}, \quad (11)$$

where (*l-1*) is top layer, and (*l*) is the bottom layer.

The azimuthally-variant residuals were auto-picked and applied to the COV gathers. Figure 8 shows the gathers before applying the residual traveltimes (left) and after applying them (right). A sequence of white and yellow backgrounds indicate offset. Offset changes where background color changes. The Mahogany bench time picks from stacked data is indicated by light green on the pre-stack COV gather. It can be seen that the flatness of

Mahogany bench is significantly improved after the application residual travel times, especially at larger offsets.

For one COV gather, azimuthally-variant traveltime residuals are plotted as function of increasing azimuth in Figure 9. Traveltime residuals mostly indicate a fast velocity direction in the northwest direction around 22º NE. Those residuals used to calculate traveltimes in equation (8).
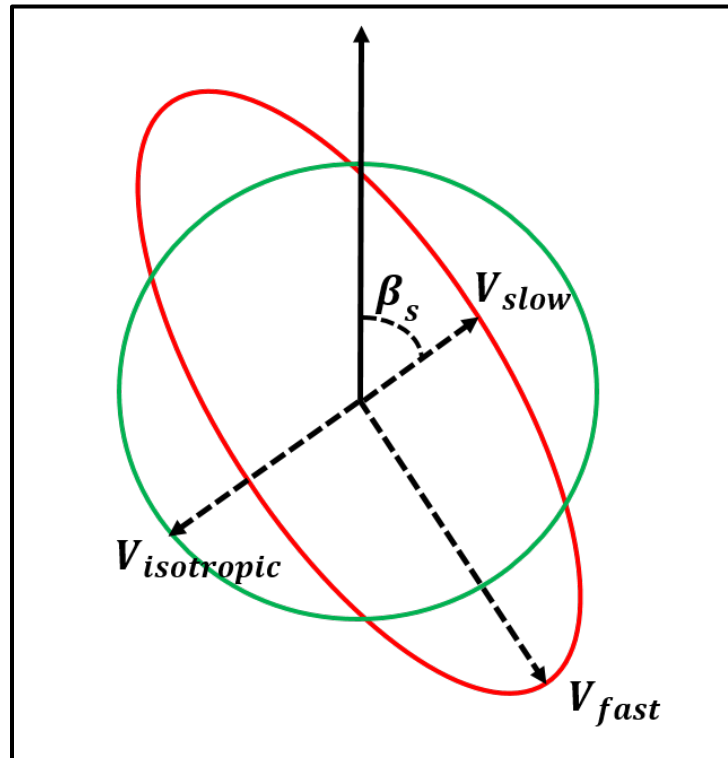

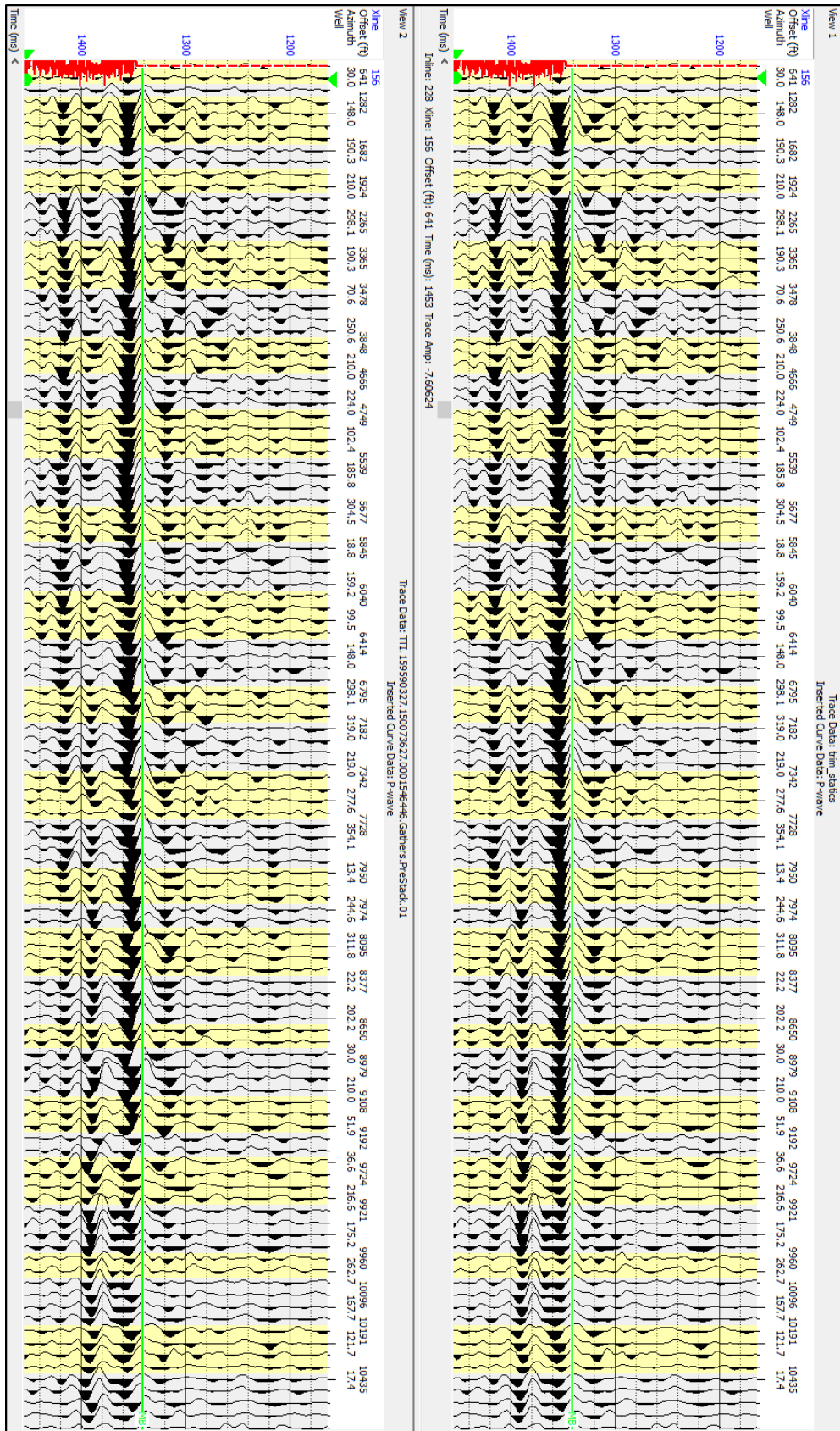Fig. 7. Isotropic RMS velocity vs azimuthally variant RMS velocity.

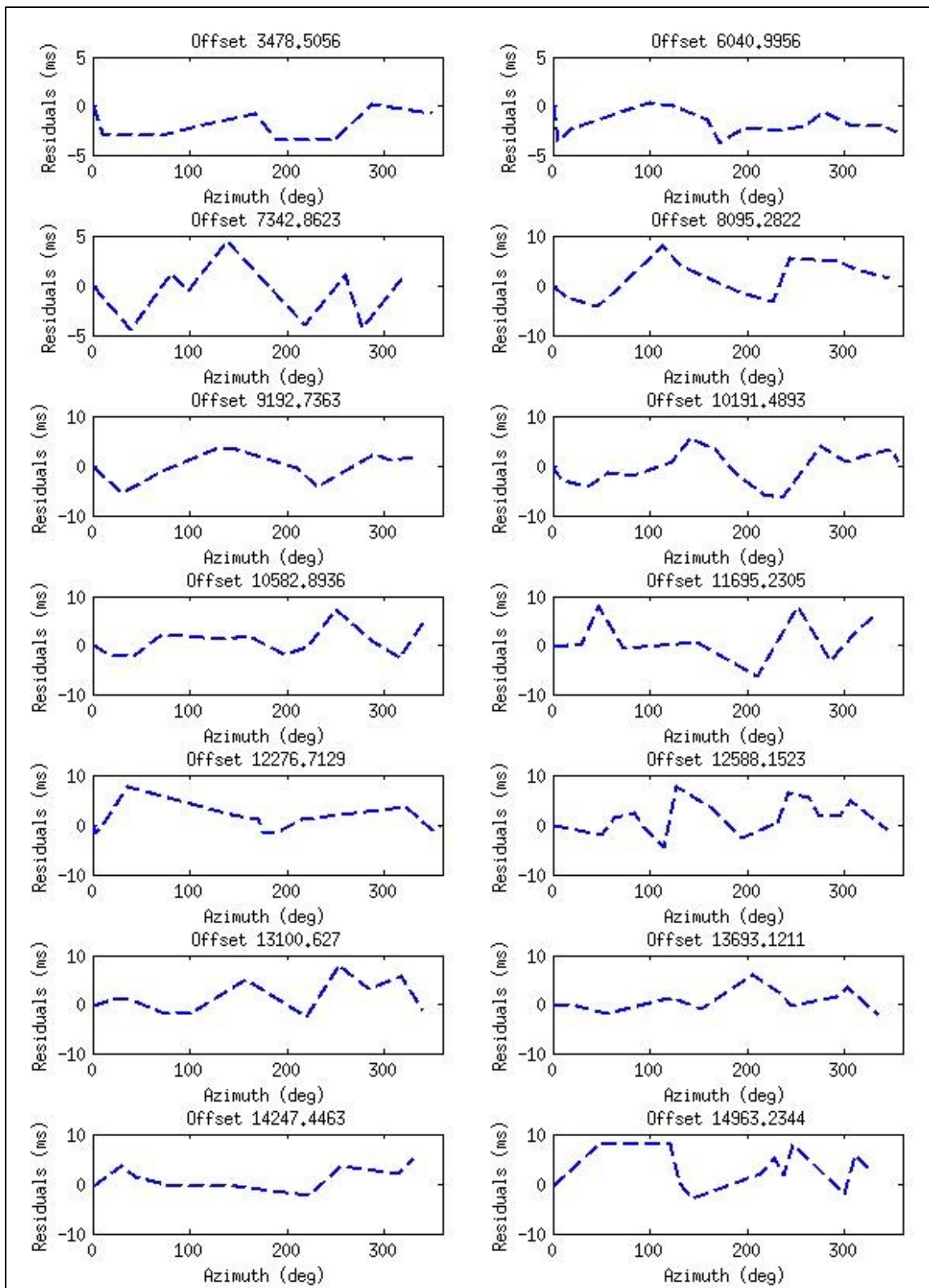Fig 8. COV Gathers: Before (left) and after (right) applying azimuthal residuals.

Fig 9. Traveltime residuals for a COV gather as function of increasing azimuth. Traveltime residuals mostly indicate a fast velocity direction in the northwest direction around 220°.

RESULTS

Fast RMS velocity, slow RMS velocity, and their directions were calculated for all horizons. Then, from those three velocities, a velocity anisotropy percentage was calculated by dividing the difference between the fast and slow RMS velocities by the slow RMS velocity. Ellipse coefficients were inverted for top and base of each reservoir. From the two sets of ellipse coefficients, Dix-type interval coefficients were calculated as described by Equation (7). From those coefficients, fast, slow interval velocities, and their directions are calculated to estimate the interval velocity anisotropy orientation and percentage. Figure 10 shows interval fast velocity direction for the overburden, Upper Green River Formation, Lower Green Formation, and Wasatch.

Rickman et. al. (2008) defined a relationship between brittleness and Young's modulus and between brittleness and Poisson's ratio. Higher Young's modulus implies higher brittleness, and higher brittleness implies a higher ability of the rock to break under stress. In order to obtain geomechanical attributes, a pre-stack elastic inversion workflow was applied to estimate Young's modulus, Poisson's ratio, and density. For the AVO inversion, six wells were used. Figure 12 shows geomechanical attributes for Upper Green River formation. Those attributes are brittleness derived from inverted Poisson's ratio (left) and brittleness derived from inverted Young's modulus (right). The geomechanical attributes correlate well with each other. Figure 13 shows a time slice of coherency post-stack attribute across the Upper Green River formation. The coherency attribute can be used to detect structural discontinuities in seismic data and sharp lithologic changes.

CONCLUSIONS AND FUTURE WORK

For the development of unconventional reservoirs, azimuthal variations of P-wave velocities can be a valuable tool for fracture information. In this paper, we have implemented a VVAZ workflow for 3D pre-stack seismic data from Altamont-Bluebell field. We think that the use of Dix-type interval coefficients has an advantage over the use of coefficients obtained from RMS velocities for a single layer because it makes VVAZ less sensitive to overburden properties. Therefore, we have applied a Dix-type interval technique to the three main reservoir. Finally, we have estimated some geotechnical and coherency attributes.
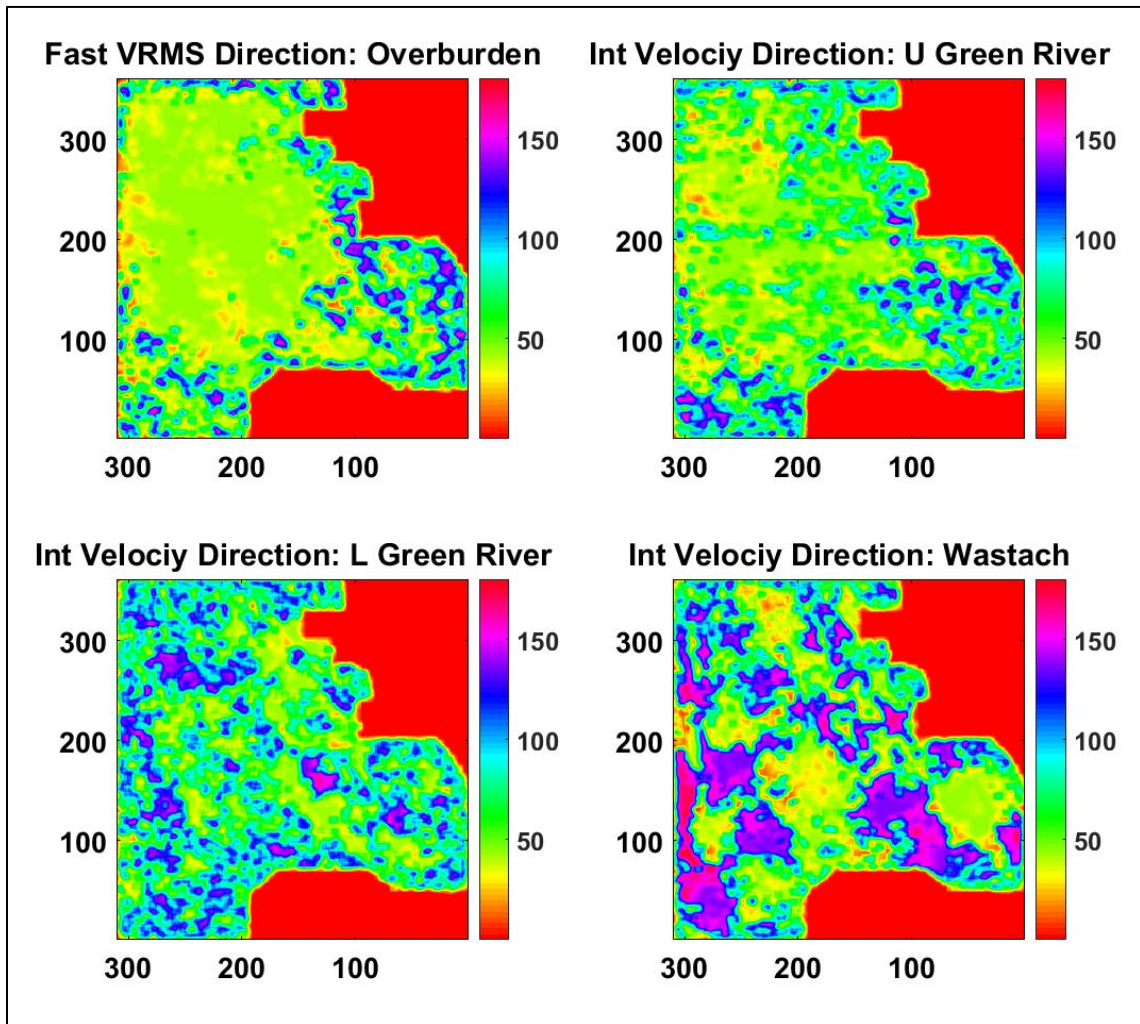
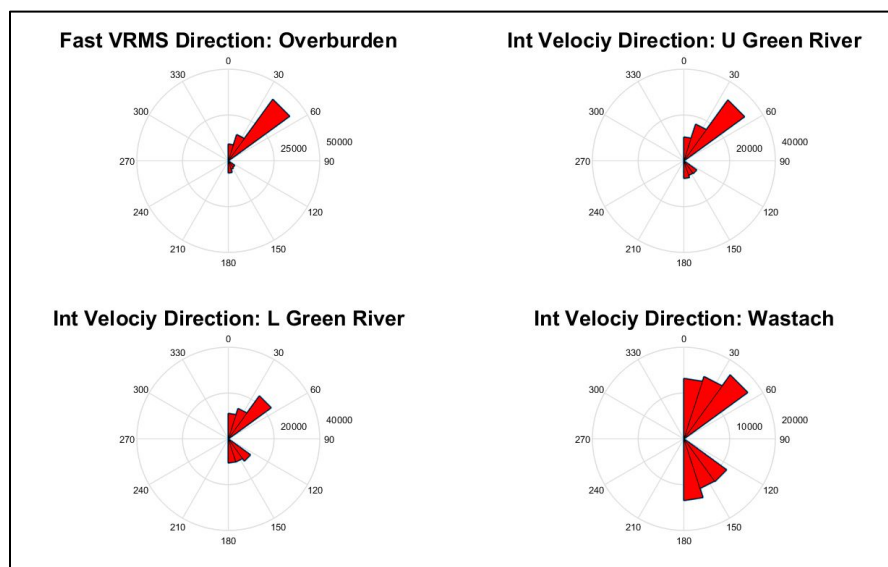Fig. 10. Interval fast velocity direction for: overburden, and three reservoirs.

Fig. 11. Circular histogram of Interval fast velocity direction for: overburden, and three reservoirs.

Fig. 10. Isotropic RMS velocity vs. fast RMS velocity vs. slow RMS velocity in (1000 ft/s).
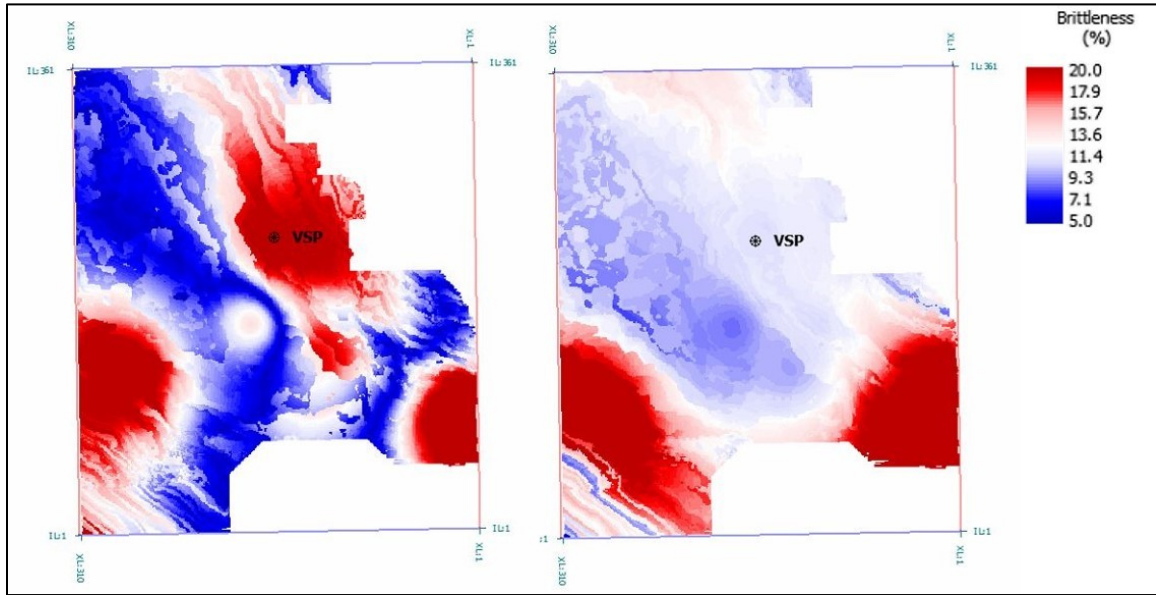

Figure 12. Geomechanical attributes for Upper Green River formation: brittleness derived from inverted Poisson's ratio (left) and brittleness derived from inverted Young's modulus (right).
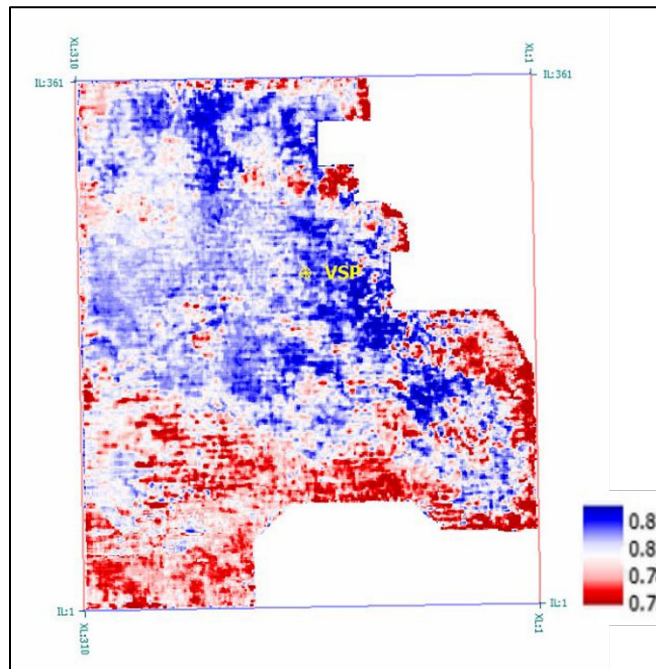

Figure 13. Coherency attribute for Upper Green River formation

ACKNOWLEDGEMENTS

REFERENCES

Adams, C., 2014, Ministry of Natural Gas Development: Northeast BC Activity Update.

Al Dulaijan, K., G. Margrave and J. Wong, 2015, 3D seismic physical modeling for azimuthal variations of P-wave velocity: CREWES Research Report.

CGGVeritas, 2014, Hampson-Rusell Software Manual: Release 9.

Grechka, V., & Tsvankin, I., 1998, 3-D description of normal moveout in anisotropic inhomogeneous media. Geophysics, 63(3), 1079-1092.

Grechka, V., Tsvankin, I., & Cohen, J. K., 1999, Generalized Dix equation and analytic treatment of normal-moveout velocity for anisotropic media. Geophysical Prospecting, 47(2), 117-148.

Jenner, E., 2001, Azimuthal anisotropy of 3-D compressional wave seismic data, Weyburn Field, Saskatchewan, Canada: Ph.D. thesis, Colorado School of Mines.

Lucas, P. T., & Drexler, J. M.,1976, Altamont-Bluebell--a major, naturally fractured stratigraphic trap, Uinta basin, Utah.

Lynn, H. B., Bates, R., Layman, M., & Jones, M. ,1995, Natural fracture characterization using P-wave reflection seismic data, VSP, borehole imaging logs, and the in-situ stress field determination. In Low Permeability Reservoirs Symposium. Society of Petroleum Engineers.

Morgan, C. D., 2003, Geologic Guide and Road Logs of the Willow Creek, Indian, Soldier Creek, Nine Mile, Gate, and Desolation Canyons, Uinta Basin, Utah (OFR-407).

Morgan, Craig D., J. Wallace Gwynn, M. Lee Allison, Richard Curtice, Milind D. Deo, Richard Jarrard, Thomas H. Morris, and Carol N. Tripp., 2003, Characterization of the Bluebell Oil Field, Uinta Basin, Duchesne and Uintah Counties, Utah (SS-106 Pt. 1).

Rickman, R., Mullen, M., Petre, E., Grieser, B. and Kundert, D., 2008, A practical use of shale petrophysics for stimulation design optimization: all shale plays are not clones of the Barnett Shale. SPE 115258.

Rüger, A., 2001, Reflection coefficients and azimuthal AVO analysis in anisotropic media. Society of Exploration Geophysicists.